On the phase-field modelling of solute trapping during rapid solidification

Thesis submitted to

Indian Institute of Science, Bangalore

in partial fulfilment for the award of the degree of

Bachelor of Science(Research)

in

Materials Science

by

Bikramjit Karmakar

(11-01-00-10-91-15-1-12503)

Under the supervision of

Dr. Abhik Choudhury

UG Programme

Indian Institute of Science, Bangalore

Spring Semester, 2018-19

April, 2019

DECLARATION

I certify that

(a) The work contained in this report has been done by me under the guidance of my supervisor.

(b) The work has not been submitted to any other Institute for any degree or diploma.

(c) I have conformed to the norms and guidelines given in the Ethical Code of Conduct of the Institute.

(d) Whenever I have used materials (data, theoretical analysis, figures, and text) from other sources, I have given due credit to them by citing them in the text of the thesis and giving their details in the references.

Date: April 26, 2019   (Bikramjit Karmakar)

Place: Bangalore   (11-01-00-10-91-15-1-12503)

UG PROGRAMME

INDIAN INSTITUTE OF SCIENCE, BANGALORE

BANGALORE - 560012, INDIA

CERTIFICATE

This is to certify that the project report entitled "**On the phase-field modelling of solute trapping during rapid solidification**" submitted by **Bikramjit Karmakar** (Sr No. 11-01-00-10-91-15-1-12503) to Indian Institute of Science, Bangalore towards partial fulfilment of requirements for the award of degree of Bachelor of Science(Research) in Materials Science is a record of bona fide work carried out by him under my supervision and guidance during Spring Semester, 2018-19.

<div style="text-align: right">

Dr. Abhik Choudhury

Materials Engineering

Indian Institute of Science, Bangalore

Bangalore - 560012, India

</div>

Date: April 26, 2019

Place: Bangalore

Abstract

Rapid solidification is a phenomenon occurring under conditions that are far from equilibrium, and one of the manifestations of it is solute trapping. Solute trapping is used to define a process of solute redistribution at the interface, quantified by an increase in the partition coefficient from its equilibrium value towards unity. Rapid solidification forms an important processing technique and modelling it bears significant technological importance in designing materials and processes The first phase-field studies of solute trapping were done by Wheeler et. al, where they showed the solute trapping phenomenon being naturally contained in the phase field equations. We reproduce this study and address its limitation by modifying the flux to the hyperbolic type.

We also show how solute trapping is naturally contained in the grand potential based phase field model. To simulate the steady-state solutions we modify the obstacle based potential to a double-well based potential in the model. The grand potential model (GP) is used to show the chemical potential jump at the interface at higher velocities. Solving for independent chemical potential also allows us to evaluate the solid and liquid composition independently, which is used to show change in trapping behaviour based on the definition of partition coefficient. We also show how the behaviour is affected by the choice of mobility interpolation function at the interface and relevant discussion is also presented. A comparison of the results obtained from GP and WBM is presented.

In the end, we present high-velocity asymptotics for the chemical potential and use this to verify our simulations, find the dependency of interface and determine the characteristic velocity V_{DI}

Acknowledgements

Contents

List of Figures

List of Tables

Symbols

ϕ	phase field variable
c	overall composition
c^S	solid composition
c^L	liquid composition
D^S	solid diffusivity
D^L	liquid diffusivity
μ	chemical potential
M_ϕ	phase field mobility
δ	interface width
k_E	equilibrium partition coefficient
$k(V)$	non-equilibrium velocity dependent partition coefficient
σ	surface energy
V	velocity of the solidification front
V_{DI}	characteristic velocity for non-equilibrium
V_D	characteristic velocity for complete diffusionless transformation
m_L	Liquidus slope
c_∞	farfield composition
R	gas constant
T	Operating temperature of directional solidification
T_m	melting temperature of the solid
v_m	molar volume
h_α	interpolation function

Chapter 1

Introduction

The primary purpose of computational modeling is to gain a deeper understanding of experimental systems and use this understanding to improve technology. A secondary goal of computer modeling is to generate a new insight by predicting complex experimental observations accurately. The specific motivation of this work was to model the phenomena of solute trapping occurring at high solidification rates. Rapid Solidification is a non-equilibrium phenomena, the dynamics of which is extremely difficult to study experimentally. The phase-field method, which is described in detail in the rest of this work is perhaps the best tool available to understand the complexity of the problem. Although the phase-field method has been developed well in the near-equilibrium regime, limited progress has been made to use it to understand what happens when the systems in contact are far from equilibrium. The work done here is an attempt to study, modify, and point out limitations of the existing work which opens the possibility to study complex problems like dendritic solidification etc. at high solidification rates.

1.1 Basics of the phase field method

Phase-field modelling has become major part of computational materials science since it is the natural way to use the thermodynamic data to study the kinetics of the microstructural evolution. Phase field method has been used to study a variety of problems which includes phase transitions, directional solidification, nucleation and spinodal decompostion, grain growth, dendritic growth etc.[7, 8] It is essentially based on the idea that microstructural interfaces are diffuse at nanoscale and can be represented by smoothly varying order parameter. Phase-field implicitly incorporates curvature-driven physics and handles interface creation which is hard to capture with a sharp interface model. Also, the phase-field equations capture behavior occurring in the bulk away from interfaces making it ideally suited for modeling the complex morphologies that arise in the microstructure study.

Evolution equations for the order parameters are found by applying a variational approach to the free energy functional. When the time derivative is set equal to the divergence of a flux, evolution is governed by the Cahn-Hilliard equation, which applies to conserved order parameters such as composition as in Eq. (1.1)

$$\frac{\partial c}{\partial t} = \nabla \cdot \left(M(c) \nabla \frac{\delta F}{\delta c} \right) \tag{1.1}$$

Setting the time derivative equal proportional to the variational derivative yields the Allen-Cahn equation. This equation does not conserve ϕ and can be used to model phase order parameters:

$$\frac{\partial \phi}{\partial t} = -M(\phi) \frac{\delta F}{\delta \phi} \tag{1.2}$$

1.2 Rapid Solidification and Solute Trapping

Rapid solidification is a phenomenon occurring under conditions that are far from equilibrium, and one of the manifestations of it is solute trapping. The term "Solute

trapping" is used to define a process of solute redistribution at the interface which is accompanied by a jump in chemical potential at the interface when described in terms of sharp-interface models and is quantified by an increase in the partition coefficient(k) from its equilibrium value(k_e) towards unity [13]. Rapid solidification forms an important processing technique and modelling it bears significant technological importance in designing materials and processes. Rapid solidification products accompanying solute trapping include wires and foils which can be used in powder metallurgy or in producing higher-performance composite materials.

1.3   Literature Review

Solute trapping has been studied both theoretically and experimentally. Theoretical studies include analytical models[4, 13, 20], phase-field model [2, 11], MD and MC computer simulations [1, 10, 23]. All of these studies are centred around investigating how the partition coefficient reaches unity with the increase in velocity. A more detailed discussion is done in the next section.

In experimental studies related to rapid solidification, Olsen and Hultgren and Duwez et al. first observed a complete solute trapping leading to diffusionless (partitionless) solidification [19]. They showed that rapidly solidifying alloy systems lead to the originating of supersaturated solid solution with the initial chemical composition of the alloy. Later on, crystal microstructures with the initial chemical composition were found by Biloni and Chalmers in rapidly solidified pre-dendritic and dendritic patterns [6]. More experimental investigation by Baker and Cahn [5], Miroshnichenko[18] and Eckler *et al.* [12] show that the effect of solute trapping is more pronounced with increasing driving forces for solidification.

1.4 Overview of analytical and computational models for solute trapping

1.4.1 Continuous growth model by Aziz and Kaplan

The continuous growth model (CGM) by Aziz and Kaplan [4] is one of the first and by far the most celebrated model to account for solute trapping and related phenomena. It is a model based on forward and reverse fluxes across the interface region using chemical reaction theory. At high solidification rates, atom can be trapped at high-energy lattice site of the crystal lattice which leads to non-equilibrium at the interface. This leads to formation of metastable solids. In CGM, partition coefficient as a function of solidification velocity(V) is related as:

$$k(V) = \frac{k_e + V/V_{DI}}{1 + V/V_{DI}} \qquad (1.3)$$

The above equation shows that the partition coefficient(k) reaches unity only when $V = \infty$. This doesn't conform with the experimental results which predicts the same for a finite velocity. To amend this, partition coefficient was redefined by Sobolev[20] as

$$k(V) = \frac{\left(1 - V^2/V_D^2\right)k_e + V/V_{DI}}{1 - V^2/V_D^2 + V/V_{DI}}, \quad V < V_D$$
$$k(V) = 1, \quad V \geqslant V_D \qquad (1.4)$$

1.4.2 The Wheeler-Boettinger-McFadden(WBM) phase field model and solute trapping in it

Wheeler, Boettinger, and McFadden [22] simulated isothermal phase transitions in binary alloys in what became known as the 'classic' (WBM) two phase model. The model in based on the Helmholtz free energy functional. The first phase-field studies of solute trapping were done by Wheeler et. al, where they showed the solute trapping phenomenon being naturally contained in the phase field equations

essentially arising out of gradient flow thermodynamics. Wheeler obtained that the partition coefficient approaches unity asymptotically at high interface velocity. The results of Wheeler et al. was similar to the results of CGM which essentially forms the starting point of our study.

1.4.3 Trapping in low-interface velocity and the anti-trapping current

KKS in [15] showed the trapping can occur in low interface velocities by varying M_ϕ, which essentially changes the composition at the interface.It is also important to emphasise that, the trapping effect also comes as an artifact at low solidification rates for which Karma and coworkers[14] proposed the anti-trapping current to reduce, and perhaps remove the effect of trapping in low interface velocity simulation. However, for our case, trapping is an experimentally verified phenomenon occurring at high solidification rates.

The Anti-trapping current is also of interest because of its ability to control trapping. Thus one could perhaps hypothesise to control trapping by controlling the anti trapping current. However such an hypothesis would be debunked owing to the fact that anti-trapping current is derived for low driving forces, and is valid only for that regime. The driving force during trapping is extremely high.

1.5 Organisation of the thesis

In Chapter 2,we reproduce the work of Wheeler et al.[2] showing that the partition coefficient (k) approaches unity asymptotically with an increase in velocity, essentially meaning $k \to 1$ when $V \to \infty$. However, the experiments show this for a finite velocity $V = V_D$. To accommodate this, in Chapter 3, we modify the phase field equations of the WBM1 using a flux of the hyperbolic type, based on the works

of Galenko and Sobolev. We simulate the steady-state solution of these modified phase-field equations to show that partition coefficient $(k) = 1$ for a finite velocity V_D. We run the simulations for two alloy systems – Cu-0.07Ni and Si-0.03As..

In chapter 4 we go on to show how solute trapping is naturally contained in the grand potential based phase field model. To simulate the steady-state solutions we modify the obstacle based potential to a double-well based potential in the model. The GP model solves for the independent chemical potential and the steady-state solutions of this shows a chemical potential jump at the interface at higher velocities. This also allows us to evaluate the solid and liquid composition independently, which is used to show change in trapping behaviour based on the definition of partition coefficient. We also show how the behaviour is affected by the choice of mobility interpolation function at the interface. A comparison of the results obtained from GP and WBM1 are presented.

In Chapter 5 we present high-velocity asymptotics for the chemical potential to compare with our simulations.

Chapter 2

Solute Trapping in WBM Model

Here we present a brief mathematical description of the model followed by the simulation results.

2.1 Wheeler-McFadden-Boettinger model

The WBM1 model is based on the Hemlmoltz free-energy functional given by [22]

$$\mathcal{F} = \int_\Omega \left[f(\boldsymbol{\phi}, c, T) + \frac{\epsilon^2}{2}|\nabla\phi|^2 \right] dV \tag{2.1}$$

where Ω is the volume of the system and the ϵ the gradient energy coefficient is assumed to be a constant. The phase-field order parameter ϕ is 1 in solid and 0 in liquid. The free energy density $f(\phi, c, T)$ in terms of bulk solid and liquid free energies f_S and f_L is written as

$$f(\phi, c, T) = p(\phi)f_S(c, T) + \{1 - p(\phi)\}f_L(c, T) + \frac{W(c)}{4}g(\phi) \tag{2.2}$$

where

$$g(\phi) = \phi^2(1 - \phi)^2, \quad p(\phi) = \phi^2(3 - 2\phi) \tag{2.3}$$

7

$g(\phi)$ is a double-well type potential and $W(c)$ is the parameter related to surface energy and interface thickness by,

$$\epsilon^2 = 6\sigma_A l_A, \quad W_A = 12\sigma_A/l_A \tag{2.4}$$

where σ_A is the surface energy and l_A is the interface width. . (2.2) can be alternatively written as

$$f(\phi, c, T) = cf_B(\phi, T) + (1 - c)f_A(\phi, T) + \frac{RT}{v_m}I(c) \tag{2.5}$$

where,

$$\begin{aligned}
f_j(\phi, T) &= W_j \int_0^\phi u[u - 1]\left[u - 1/2 - \beta_j(T)\right] du \\
&= \frac{W_j}{4}g(\phi) + \frac{W_j\beta_j(T)}{6}p(\phi)
\end{aligned} \tag{2.6}$$

Thus, the undercooling can be related as

$$\frac{W_A\beta_A(T)}{6} = L_A\frac{(T - T_A)}{T_A} \tag{2.7}$$

The governing equations using (1.1) and (1.2) are [22] -

$$\frac{\partial \phi}{\partial t} = M_1\left[\epsilon^2\nabla^2\phi - \left(c\frac{\partial f_B}{\partial \phi} + (1 - c)\frac{\partial f_A}{\partial \phi}\right)\right] \tag{2.8}$$

$$\frac{\partial c}{\partial t} = M_2\nabla \cdot [c(1 - c)\nabla(f_B - f_A)] + D\nabla^2 c \tag{2.9}$$

In a moving co-ordinate frame of reference with constant velocity V, Eq(2.7) and Eq(2.8) becomes [2]

$$\frac{-V}{M_1}\frac{d\phi}{dz} = \epsilon^2\frac{d^2\phi}{dz^2} - \frac{\partial f}{\partial \phi}(\phi, c, T) \tag{2.10}$$

$$-V(c - c_S) = c(1 - c)M_2\frac{d}{dz}\left[\frac{\partial f}{\partial c}(\phi, c, T)\right] \tag{2.11}$$

The diffusivity(D) and mobility(M_2) are related by

$$D = M_2 \frac{RT}{v_m} \tag{2.12}$$

Across the interface the D is interpolated as

$$D(\phi) = D_S r(\phi) + D_L[1 - r(\phi)] \tag{2.13}$$

where $r(\phi)$ is the interpolation function.

2.2 Simulation and results

We use finite difference method for discretization, and solve the equations implicitly. The non-linear equation solver $fsolve$ in *octave* is used to solve the set of non-linear equations equations. The c and ϕ solutions were converged iteratively with a tolerance of 10^{-12}

We used $r(\phi) = \phi$. For ϕ we fix the value of 1 and 0 for solid and liquid ends respectively. For c we fix c_∞ as the far field composition on the solid side and use a no flux boundary condition for the liquid side.

The partition coefficient k is defined as (as used by Wheeler et al[2])

$$k = \frac{c_\infty}{c_{\max}} \tag{2.14}$$

There are other choices of partition coefficient in the literature and definition of which plays an important role in the results. A detailed discussion on this is dealt in a later chapter.

The material and simulation parameters are summarised below.

TABLE 2.1: Thermophysical and Simulation data for Cu-0.07Ni [2, 22]

L_A	2350 J cm^{-3}
L_B	1725 J cm^{-3}
T_A	1728 K
T_B	1358 K
σ_A	2.8×10^{-5} J cm^{-2}
σ_B	2.8×10^{-5} J cm^{-2}
D_L	10^{-5} cm^2 s^{-1}
D_S	10^{-10} cm^2 s^{-1}
l_A	6.48×10^{-8} cm
l_B	6.48×10^{-8} cm
k_E	0.7965
c_∞	0.0717441
m_L	-310.9 K
M_ϕ	4.9×10^5
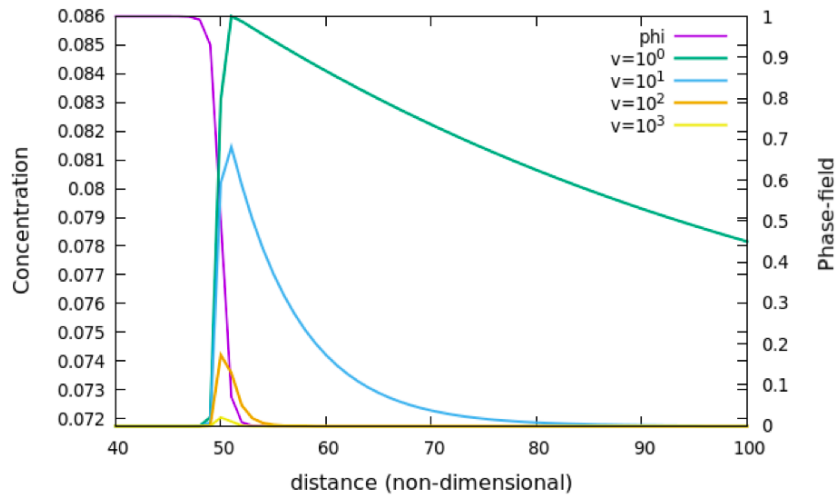
FIGURE 2.1: Composition profile at different solidification velocities for Cu-0.07Ni using WBM
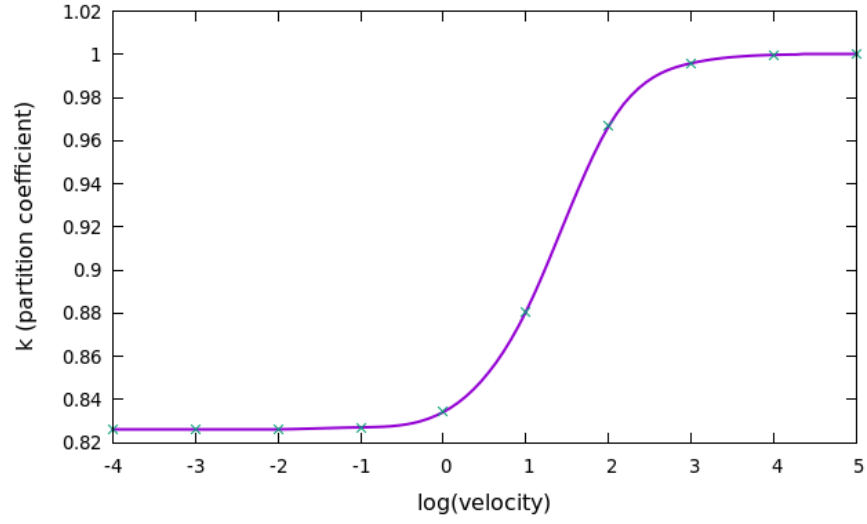
FIGURE 2.2: Variation in the partition coefficient as a function solidification velocity in Cu-0.07Ni using WBM

TABLE 2.2: Thermophysical and Simulation data for Al-0.03Si [11]

L_A	4114.754 J cm^{-3}
L_B	2270.49 J cm^{-3}
T_A	1685 K
T_B	1104 K
σ_A	4.77$\times 10^{-5}$ J cm^{-2}
σ_B	4.77$\times 10^{-5}$ J cm^{-2}
D_L	1.5$\times 10^{-5}$ cm^2 s^{-1}
D_S	3$\times 10^{-9}$ cm^2 s^{-1}
l_A	1.875$\times 10^{-7}$ cm
l_B	1.875$\times 10^{-7}$ cm
c_∞	0.03
M_ϕ	8.77$\times 10^7$
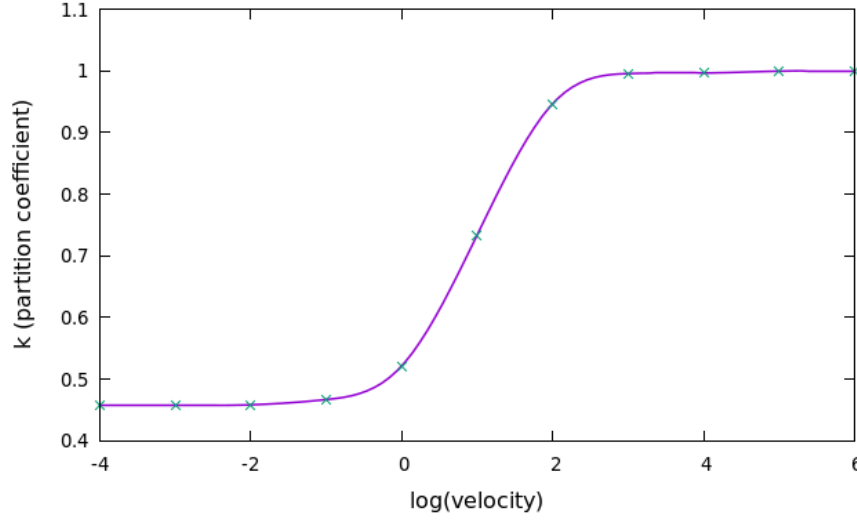
FIGURE 2.3: Variation in the partition coefficient as a function solidification velocity in Si-0.03As using WBM

2.3 Discussion

As can be seen in the Figure 2.1 an increase in velocity changes the interface composition, essentially driving it into non-equilibrium. Each of these steady state simulations are used to find the partition coefficient at that velocity using Eq(2.14). This non-equilibrium partition coefficient is then plotted as a function of velocity which is shown in Figure 2.2. These results are essentially reproduction of work done by Wheeler et al [2]. However we have also simulated Si-0.03As system for which certain experimental data is available [11] following the same methodology and plotted the variation in partition coefficient in Figure 2.3.

Although the partition coefficient seems to have become unity in the plots Fig2.2 and Fig2.3 and , it essentially approaching unity asymptotically and doesn't reach one completely. This precisely is the prediction of Aziz's model[4]. However, as mentioned in previous chapter, partition coefficient becoming unity for a finite velocity is supported by experiments. This is incorporated in the next chapter by using a hyperbolic flux.

Chapter 3

Modified WBM using hyperbolic flux

3.1   Introduction to hyperbolic flux

Diffusion flux is a number of molecules that move through a unit area plane per unit time. Net flux is due to the difference between the flow from one side of the plane and the flow from the other side of the plane. The flux from left side of the plain is proportional to $C(x-l)vdt/6$ and the flux from right side of the plain is proportional to $C(x+l)vdt/6$, where C is the particle concentration, v is the particle mean velocity. It should be noted that a particle comes to a point x at a time moment $t + \tau$ from a point $(x - l)$ or $(x + l)$ where it was at a time moment t. This essentially means that there is a time lag τ between the diffusion flux and the particle concentration (and its derivatives), where τ is relaxation time to local equilibrium (for gases it is of the order of the mean collision time). In a one dimensional case one can obtain [21]

$$J(t + \tau, x) = \frac{1}{2}(C(t, x - l) - C(t, x + l))v \tag{3.1}$$

This equation can be expanded in the form of Taylor series with two small parameters l and τ [21]

$$\sum_{n=0} \frac{\tau^n}{n!} \frac{\partial^n J}{\partial t^n} = -v \sum_{k=0} \frac{l^{2k+1}}{(2k+1)!} \frac{\partial^{2k+1} C}{\partial x^{2k+1}} \tag{3.2}$$

At $n = k = 0$ this boil down to the classical fick's law

$$J = -D \frac{\partial C}{\partial x} \tag{3.3}$$

However, such an approximation is only valid for relatively slow processes, for which, $\tau << t_0$ where t_0 is the characteristic time for the process under consideration. In the expansion of higher order we can get,

$$\tau_D \frac{\partial^2 J}{\partial t^2} + \frac{\partial J}{\partial t} = D \frac{\partial^2 J}{\partial x^2} \tag{3.4}$$

This equation is essentailly the hyperbolic flux equation which is analogous to the evolution equation for heat flux known as the Cattaneo-type equation[17]. This can be re-written as a steady state equation using diffusive velocity V_D where $V_D = \sqrt{\frac{D}{\tau}}$

$$D \left(1 - \frac{V^2}{V_D^2} \right) \frac{d^2 J}{dx^2} + V \frac{dJ}{dx} = 0 \tag{3.5}$$

Using the results by Galenko [13] we can write the steady state flux equation in terms of difference in chemical potential as

$$J = -D \left(\frac{\partial(\Delta\mu)}{\partial c} \right)^{-1} \left[1 - \frac{V^2}{V_D^2} \right] \frac{d(\Delta\mu)}{dx}, \quad V < V_D$$
$$J = 0, \quad V \geqslant V_D \tag{3.6}$$

This is precisely the flux we use to modify the composition evolution equation in WBM.

3.2 Modified WBM equations

The phase-field evolution equation remains the same as Eq(2.10) however the new composition evolution equation using Eq(3.6)

$$-V\left(c - c_S\right) = c(1-c)\left[1 - \frac{V^2}{V_D^2}\right] M_2 \frac{d}{dx}\left[\frac{\partial f}{\partial c}(\phi, c, T)\right] \quad V < V_D$$
$$-V\left(c - c_S\right) = 0 \quad V \geqslant V_D$$

(3.7)

At the local equilibrium limit $V_D \to \infty$ the above equation boils down to Eq(2.11), and at $V_D \to \infty$ and $\phi = 0$ or 1 this becomes the classical diffusion equations for bulk phases.

3.3 Simulation and Results

We follow the procedure, boundary condition and thermophysical data as mentioned in Section 2.2. The results obtained here is as what was expected, and significantly different from the results obtained from unmodified WBM.
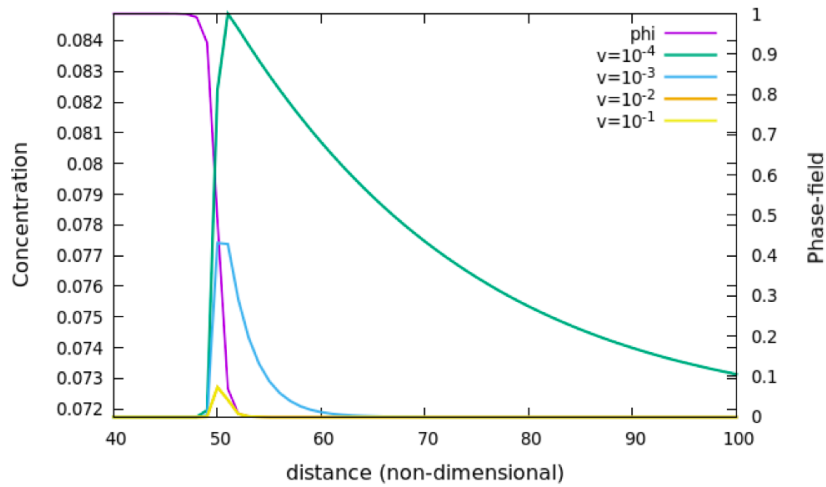
FIGURE 3.1: Composition profile at different solidification velocities for Cu-0.07Ni using hyberbolic-WBM
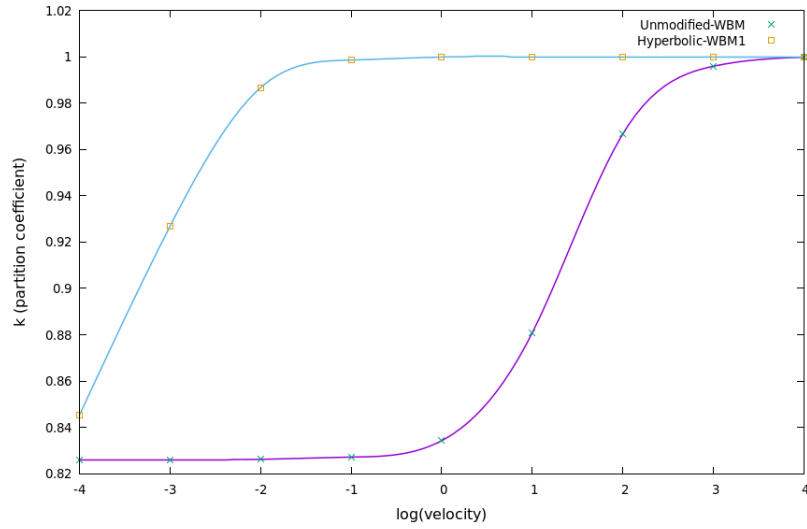
FIGURE 3.2: Comparison of partition coefficient behaviour for WBM and hyperbolic WBM of Cu-0.07Ni
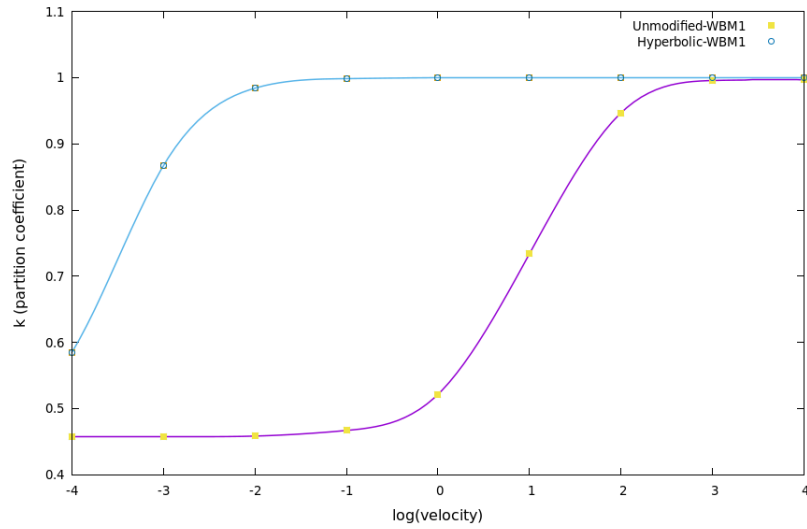
FIGURE 3.3: Comparison of partition coefficient behaviour for WBM and hyperbolic WBM of Si-0.03As

3.4 Discussion

It is shown that the model predicts complete solute trapping at the finite solidification velocity equal to the diffusion speed, $V = V_D$. This also is the condition for which the transition to completely diffusionless solidification occurs which conforms with the experimental observations [5], unlike the simulations by Wheeler.

There are similar modifications to hyperbolic type done to Darcy's law for the fluid flow in porous media, Ohm's law for the electric flux and Fourier's law for heat transfers. The validity of the hyperbolic non-fickian flux is addressed by Aurialt et. al [3] using molecular diffusion through its mechanistic Einstein definition. It was shown that such a hyperbolic description is valid, but for transient solute flows with unrealistic very small characteristic times.

In the above simulations, we have adopted the definition of partition coefficient as in Eq(2.14), which bears some concern. Partition coefficient is defined in terms of sharp interface models, where it is ratio of solid and liquid compositions at the interface. Thus the equilibrium partition coefficient is the ratio of the compositions corresponding to the common tangent construction in a free energy composition curve. To obtain the individual composition at the interface we could solve for the independent chemical potential, which is done in the next chapter using the grand-potential model [9]

Chapter 4

Trapping in Grand Potential Model

We also study how solute trapping is contained in the grand potential based phase field by Abhik [9]. The grand potential model solves for the independent chemical potential, which gives the compositions of the phases independently.

4.1 Modification to the potential type

The grand-potential is based on the obstacle type potential which gives it some computational advantages however the potential being infinite at the phase boundary makes it difficult to solve the steady-state equation implicitly. To avoid complexity we modify the phase evolution equation to a double-well potential. We use the Kobayashi's [16] notation in one dimensional form and therefore corresponding functional reads as

$$\omega = \int_\Omega \left[\Psi(\phi, \mu, T) + \frac{\epsilon}{2} |\nabla \phi|^2 \right] dV \tag{4.1}$$

For a binary alloy,

$$\Psi(\phi, \mu, T) = p(\phi)\psi_S(\mu, T) + \{1 - p(\phi)\}\psi_L(\mu, T) + \frac{\gamma}{4}g(\phi) \tag{4.2}$$

where,

$$\psi_i(\mu, T) = f_i(c_i(\mu), T) - \mu_i c_i, \quad g(\phi) = \phi^2(1 - \phi)^2, \quad p(\phi) = \phi^2(3 - 2\phi); \tag{4.3}$$

Thus the evolution equation becomes:

$$\tau\dot{\phi} = \epsilon\frac{\partial^2}{\partial x^2}\phi - \gamma\phi(1 - \phi)\left(\phi - \frac{1}{2}\right) + p'(\phi)\Delta F \tag{4.4}$$

where,

$$\Delta F = \psi_S(\mu, T) - \psi_L(\mu, T) \tag{4.5}$$

The constants can be related to the material parameters as

$$\epsilon = \sigma\delta, \quad \gamma = 72\frac{\sigma}{\delta}, \quad \tau = \frac{\delta}{M_\phi}; \tag{4.6}$$

where, δ is the interface width, σ is the surface energy and M_ϕ is the phase-field mobility.

The free energy functions we use are

$$f_L = \frac{RT}{V_m}\{c_L \ln(c_L) + (1 - c_L)\ln(1 - c_L)\} \tag{4.7}$$

$$f_S = \frac{RT}{V_m}\left\{c_S \ln(c_S) + (1 - c_S)\ln(1 - c_S) - c_S \ln(k_e) + (1 - c_S)\ln\left[\frac{1 + \frac{(T_m - T)}{m_e}}{1 + \frac{k_c(T_m - T)}{m_c}}\right]\right\} \tag{4.8}$$

The composition c_S and c_L can be written as explicit functions of μ where $\mu = \frac{df}{dc}$
Thus

$$c_S(\mu) = \frac{1}{\frac{1}{k_e Z}\exp\left(-\frac{\mu}{A}\right) + 1}, \quad c_L(\mu) = \frac{1}{\exp\left(-\frac{\mu}{A}\right) + 1}; \tag{4.9}$$

where

$$A = \frac{RT}{v_m}, \quad Z = \left[\frac{1 + \frac{(T_m - T)}{m_e}}{1 + \frac{k_c(T_m - T)}{m_c}} \right]; \tag{4.10}$$

4.2 Simulation and results

We solve the steady governing equations which are given by

$$-V\tau\frac{d\phi}{dx} = \epsilon\frac{\partial^2}{\partial x^2}\phi - \gamma\phi(1 - \phi)\left(\phi - \frac{1}{2}\right) + p'(\phi)\Delta F \tag{4.11}$$

$$-V\frac{\partial\mu}{\partial x} - \left(\frac{\partial c_S(\mu, T)}{\partial\mu}p(\phi) + \frac{\partial c_L(\mu, T)}{\partial\mu}[1 - p(\phi)]\right) =$$
$$\nabla \cdot \left[\left(D^S r(\phi)\frac{\partial c_S(\mu, T)}{\partial\mu} + D^L(1 - r(\phi))\frac{\partial c_L(\mu, T)}{\partial\mu}\right)\nabla\mu\right] \tag{4.12}$$
$$+V[c_S(\mu, T) - c_L(\mu, T)]\frac{\partial h_\alpha(\phi)}{\partial x}$$

Eq (4.12) is a steady state transform of the governing equation for μ in [9] and Eq (4.12) is a steady state transform to Eq (4.4)

We follow the procedure, boundary condition and thermophysical data as mentioned in Section 2.2. However in this case we set $\mu^S(c_\infty)$ as the far field potential in the boundary condition. The steady state composition profile is plotted in Figure 4.1 using $r(\phi) = \phi^2(3 - 2\phi)$

4.2.1 Choice of Partition coefficient

The partition coefficient is defined in terms of sharp interface models as

$$k(V) = \frac{\text{concentration in solid}}{\text{concentration in liquid}} = \frac{c_S}{c_L} \tag{4.13}$$
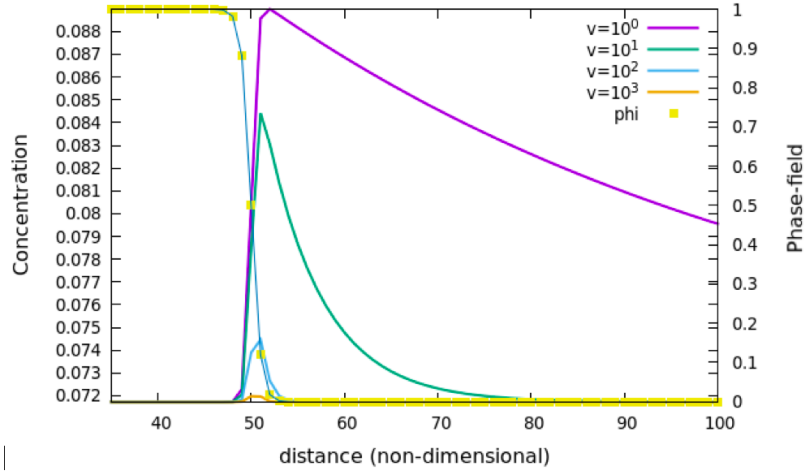
FIGURE 4.1: Composition profile at different solidification velocities for Cu-0.07Ni using GP model

There are several definitions in the literature for partition coefficient in a diffuse interface setting, which can be classified into two categories. The first one is Eq(2.14) by wheeler[2] which is

$$k_1(V) = \frac{\text{far-field concentration}}{\text{maximum of the concentration}} = \frac{c_S}{\max[c]} \tag{4.14}$$

The other one is by Danilov and Nestler [11]

$$k_D(V) = \frac{c(z_S)}{c(z_L)} \tag{4.15}$$

where z_S and z_L are positions chosen relative to the centre of interfacial zone in a systematic way with a best-fit criterion to the experimental data. Both of these definitions are based on mixture concentrations because the individual phase concentration cannot be evaluated. We adopt the definition of partition coefficient as

$$k_2(V) = \frac{c_S \text{ (far-field concentration)}}{c_L(\phi = 0.0001)} \tag{4.16}$$

$c_L(\phi = 0.0001)$ is essentially the liquid composition at the liquid side of the interface. This is shown in the Figure 4.2.
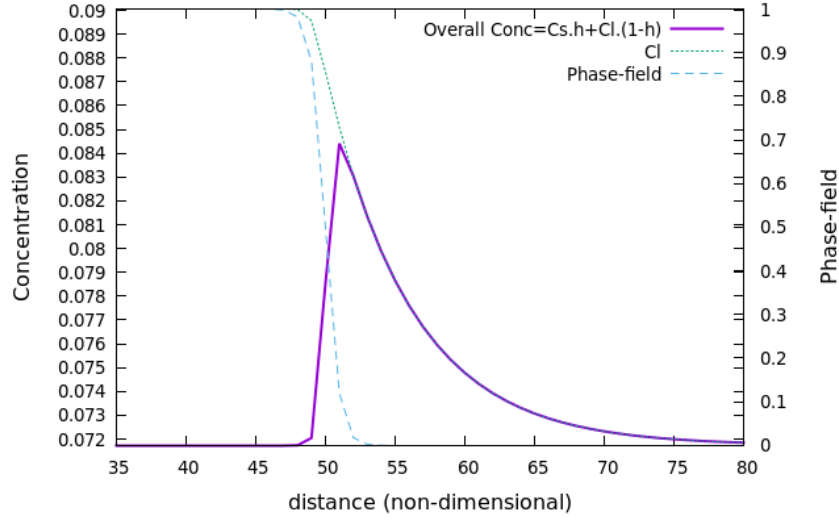
FIGURE 4.2: Liquid and overall Composition profile at velocity=10 cm/s for Cu-0.07Ni using GP model

Definition of partition coefficient in Eq(4.14) (k_1) and Eq(4.16) (k_2) is used to plot the variation in partition coefficient in Figure 4.3

FIGURE 4.3: Trapping behaviour comparison on choice of partition coefficient (k_1/k_2)

k_1 show asymptotic convergence towards unity with increasing velocity as before, however k_2 shows absolute convergence at unity for a finite velocity. Also, $k_2 = 1$

is not a criterion for completely diffusionless transformation since there exists a composition gradient inside the interface. An alternative way to quantify trapping would be to use the jump in chemical potential.

4.2.2   Jump in chemical potential

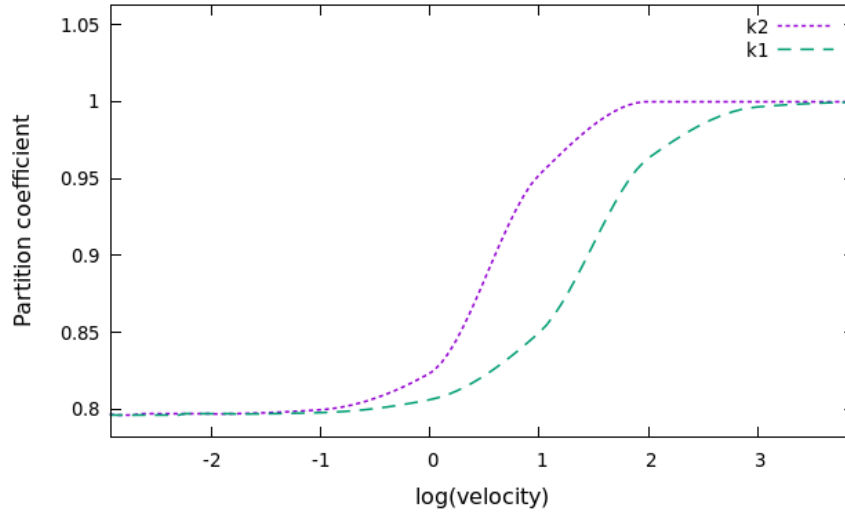As shown in Figure 4.4 the chemical potential potential on sides of the interface does not match. Thus extrapolating it to $\phi = 0.5$ can be used to quantify the jump and hence the extent of non-equilibrium. However experimental limitations prevent such a definition being used.
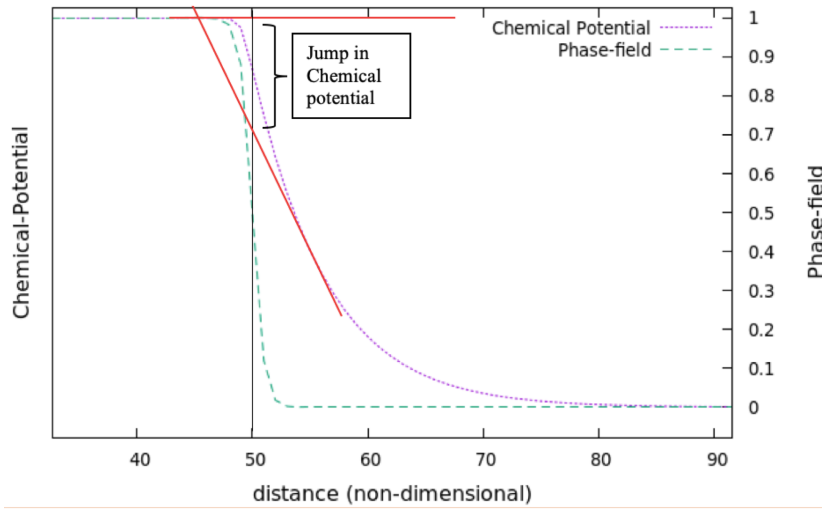
FIGURE 4.4: Jump in chemical potential at velocity=10 cm/s for Cu-0.07Ni using GP model

4.2.3   Choice of interpolation function

In a phase field model trapping also sensitive to the interpolation of diffusivity across the interface. We have performed simulations for interpolation functions - linear $r(\phi) = \phi$; square $r(\phi) = \phi^2(3 - 2\phi)$; and cubic $r(\phi) = \phi^3(10 - 15\phi + 6\phi^2)$; and have plotted it for both the choices of partition coefficient.
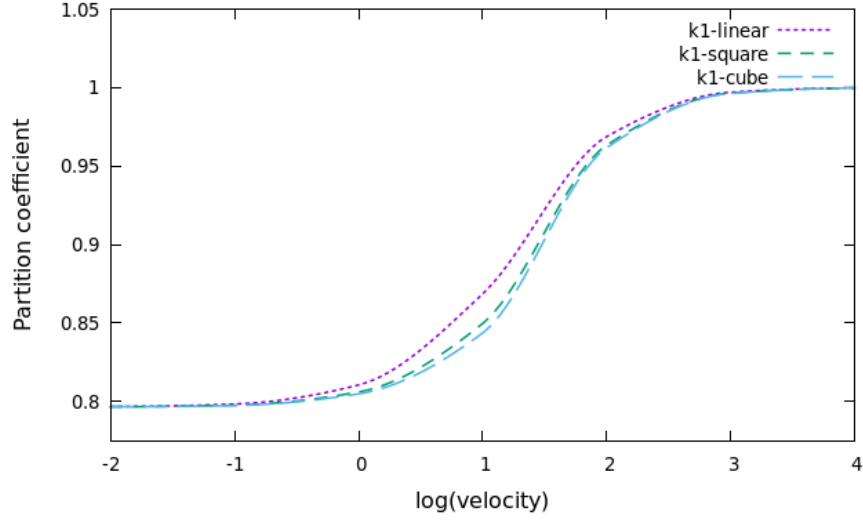
FIGURE 4.5: Trapping with different interpolation function using GP model with
$k = k_1$

As shown in the above figure the trapping behaviour differs with interpolation function with lower trapping at higher order interpolation function, for the choice of partition coefficient as k_1

However with partition coefficient as k_2 the trapping is independent of interpolation function as shown below.
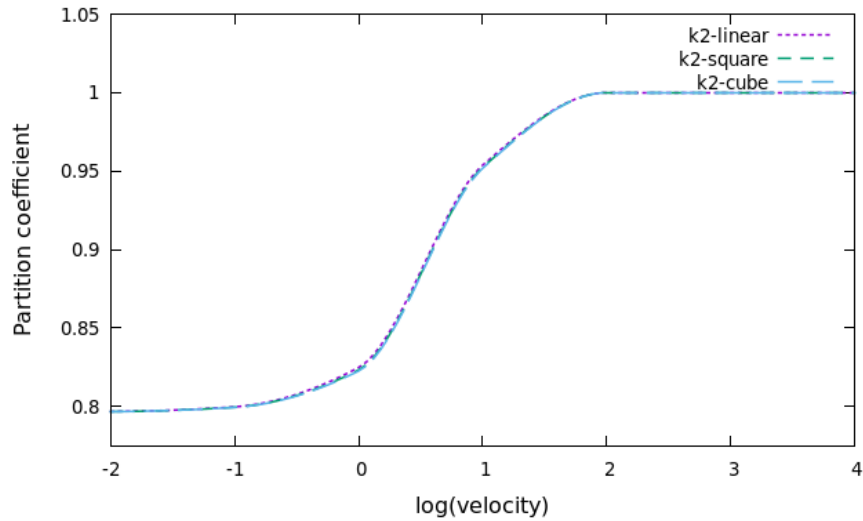
FIGURE 4.6: Trapping with different interpolation function using GP model with
$k = k_2$
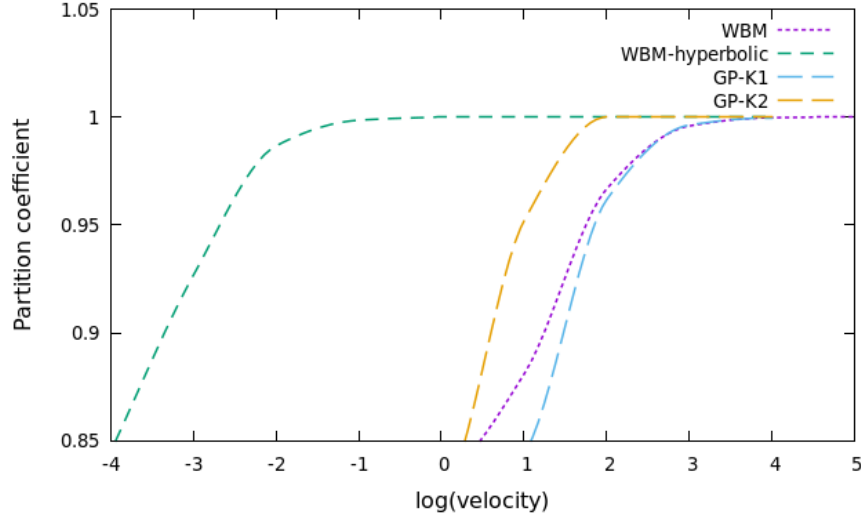
FIGURE 4.7: Comparison of trapping behaviour in GP, WBM and WBM-hyperbolic

4.3 Comparison of results

The figure above shows a comparison of trapping behaviour in different models. The WBM model and GP model with choice of partition coefficient as k_1 shows similar trapping behaviour with asymptotic convergence to unity at higher velocity. However in the regime of $k_E < k < 1$, trapping in WBM model is more than GP model. The hyperbolic WBM and GP model with choice of partition coefficient as k_2 shows absolute convergence to unity at finite velocity, with GP-k_2 being more steep. Both of them become unity at the same order of velocity, however trapping in hyperbolic-WBM being distinctly more at the same velocity in the regime of $k_E < k < 1$.

Chapter 5

High Velocity asymptotics

In this chapter we perform asymptotic analysis (using regular perturbation) of the governing equations to gain some further insight on the problem and also compare them with our simulations.

5.1 Expansion in terms of velocity

We expand the variables in terms of velocities in the form of

$$\phi = \phi^{(0)} + \frac{1}{V}\phi^{(1)} + O(1/V^2) \tag{5.1}$$

$$\mu = \mu^{(0)} + \frac{1}{V}\mu^{(1)} + O(1/V^2) \tag{5.2}$$

The solution of leading order term:$\phi^{(0)}$ using Eq(4.11)is trivial solutions of which is available in literature [2]

$$\phi^{(0)} = \frac{1}{2}\left[1 - \tanh\left(\frac{x}{\delta}\right)\right] \tag{5.3}$$

where δ is the interface thickness.

For solution of leading order $\phi^{(0)}$ we write Eq(4.12) as

$$-V \left(\frac{dc(\mu)}{dx} \right) = \nabla \cdot \left(M(D, \mu, \phi) \frac{d\mu}{dx} \right) \tag{5.4}$$

where

$$c(\mu) = c^s(\mu)h_\alpha + c^l(\mu)(1 - h_\alpha), \quad M(D, \mu, \phi) = D^s \frac{dc^s}{d\mu} h_\alpha + D^l \frac{dc^l}{d\mu}(1 - h_\alpha); \tag{5.5}$$

For free energy of the form

$$f_L = \frac{RT}{V_m} \left\{ c_L \ln(c_L) + (1 - c_L) \ln(1 - c_L) \right\} \tag{5.6}$$

$$f_S = \frac{RT}{V_m} \left\{ c_S \ln(c_S) + (1 - c_S) \ln(1 - c_S) - c_S \ln(k_e) + (1 - c_S) \ln \left[\frac{1 + \frac{(T_m - T)}{m_e}}{1 + \frac{k_c(T_m - T)}{m_c}} \right] \right\} \tag{5.7}$$

Such a choice of free energy has the equilibrium partition coefficient k_e, the melting temperature T_m and solidification temperature T as parameters. Although we have explicitly defined our choice of free energy, the parameters (k_e, T_m, T) on which it is dependent makes it fairly general in the regime of dilute solution and linear phase diagram. Also, since the functions are invertible over $(0, 1)$; individual compositions can be written as explicit functions of μ

$$c_S(\mu) = \frac{1}{\frac{1}{k_e Z} \exp\left(-\frac{\mu}{A}\right) + 1}, \quad c_L(\mu) = \frac{1}{\exp\left(-\frac{\mu}{A}\right) + 1}; \tag{5.8}$$

where

$$A = \frac{RT}{v_m}, \quad Z = \left[\frac{1 + \frac{(T_m - T)}{m_e}}{1 + \frac{k_c(T_m - T)}{m_c}} \right]; \tag{5.9}$$

Integrating (5.4) once gives,

$$-V(c(\mu) - c_\infty) = M(D, \mu, \phi) \frac{d\mu}{dx} \tag{5.10}$$

Therefore the leading order solution of this is given by -

$$c(\mu^{(0)}) = c_\infty \tag{5.11}$$

To solve this equation we use a short-hand notation where $\eta(x) = \exp(\frac{-\mu^0}{A})$

Thus,

$$\frac{1}{\frac{1}{k_e Z}\eta(x) + 1}h_\alpha + \frac{1}{\eta(x) + 1}(1 - h_\alpha) = c_\infty \tag{5.12}$$

Solving for $\eta(x)$ gives a quadratic solution -

$$\eta(x) = \frac{-b + \sqrt{b^2 - 4ac}}{2a} \tag{5.13}$$

$\eta(x) > 0$; where,

$$a = \frac{c_\infty}{k_e Z}$$

$$b = \left[c_\infty(1 + \frac{1}{k_e Z}) - h_\alpha(1 - \frac{1}{k_e Z}) - 1\right] \tag{5.14}$$

$$c = c_\infty - 1$$

This gives the solution of $\mu^{(0)}$ as

$$\mu^{(0)}(x) = -A \ln\left[\eta(x)\right] \tag{5.15}$$

The first order solution is given by

$$-V\left(c(\mu^{(0)} + \frac{1}{V}\mu^{(1)}) - c_\infty\right) = M(D, \mu^{(0)}, \phi^{(0)})\frac{d\mu^{(0)}}{dx} \tag{5.16}$$

$$c(\mu^{(0)} + \frac{1}{V}\mu^{(1)}) = \frac{1}{\frac{1}{k_e Z}\eta(x)\exp(-\frac{\mu^{(1)}}{VA}) + 1}h_\alpha + \frac{1}{\eta(x)\exp(-\frac{\mu^{(1)}}{VA}) + 1}(1 - h_\alpha) \tag{5.17}$$

The $\exp(-\frac{\mu^{(1)}}{VA})$ can be written as a Taylor series expansion giving

$$c(\mu^{(0)} + \frac{1}{V}\mu^{(1)}) = \frac{1}{\frac{1}{k_e Z}\eta(x)(1 - (\frac{\mu^{(1)}}{VA})) + 1}h_\alpha + \frac{1}{\eta(x)(1 - \frac{\mu^{(1)}}{VA})) + 1}(1 - h_\alpha) \quad (5.18)$$

Collecting coefficients of $\frac{1}{V}$ gives $\mu^{(1)}$ as

$$\mu^{(1)} = \frac{\eta(x)A}{h_\alpha\left(1 - \frac{1}{k_e Z}\right) - 1}M(D, \mu^{(0)}, \phi^{(0)})\frac{d\mu^{(0)}}{dx} \quad (5.19)$$

The remaining functions on RHS can be evaluated as

$$\frac{d\mu^{(0)}}{dx} = -\left(\frac{1}{2a}\left(\frac{b}{(b^2 - 4ac)^{0.5}} - 1\right)\right) \cdot \left(1 - \frac{1}{k_e Z}\right) \cdot h'_\alpha \cdot \frac{1}{2\delta} \cdot \text{sech}^2\left(\frac{x}{\delta}\right)$$

$$(5.20)$$

$$M(D, \mu^{(0)}, \phi^{(0)}) = D^s h_\alpha \frac{\eta(x)\mu_0}{k_e Z A\left(\frac{\eta(x)}{k_e Z} + 1\right)^2} + D^l(1 - h_\alpha)\frac{\eta(x)\mu_0}{A(\eta(x) + 1)^2}$$

5.2 Chemical potential jump

Now that we have obtained the chemical potential profile as function, we can show the jump in chemical potential. The chemical potential jump is given by

$$\Delta\mu = \lim_{\phi \to 1}\mu - \lim_{\phi \to 0}\mu \quad (5.21)$$

The chemical potential jump matches exactly with our simulations.

5.3 Interface width dependence

We can also determine the interface width dependence on the extent trapping using the asymptotic analysis.

(a) interface width $d = d_0$ (b) interface width $d = 2d_0$
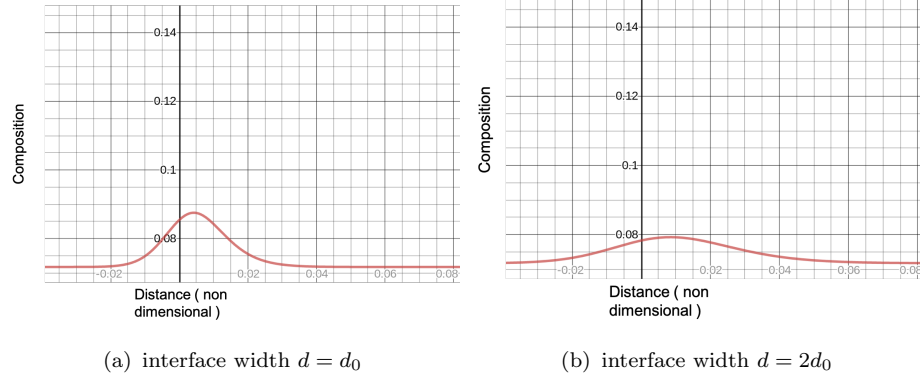
FIGURE 5.1: Trapping at different interface widths

5.4   Determination of characteristic velocity V_{DI}

Like Wheeler et al [2] we can use the results of the asymptotic analysis to determine the characteristic velocity V_{DI}. Determination of correct V_{DI} bears significance in characterizing solidification cracking during additive manufacturing.

At $k_E < k < 1$ the all solute partitioning models boils down to Aziz's [4] model

$$k = \frac{k_E + V/V_{DI}}{1 + V/V_{DI}} \tag{5.22}$$

which can be approximated by

$$k \approx 1 - (1 - k_E)\left[\frac{V_{DI}}{V}\right] + O\left(\left[\frac{V_{DI}}{V}\right]^2\right) \tag{5.23}$$

Eq (5.16) can be written as

$$c(x) = c_\infty - \frac{1}{V}\left(M(D, \mu^{(0)}, \phi^{(0)})\frac{d\mu^{(0)}}{dx}\right) \tag{5.24}$$

At $x = x_k$ depending on choice of partition coefficient, above equation becomes

$$k = 1 + \frac{1}{V} \left[\frac{1}{c(\mu(x_k))} \left(M(D, \mu^{(0)}, \phi^{(0)}) \frac{d\mu^{(0)}}{dx} \right) \right] \tag{5.25}$$

Comparing with Eq (5.23)

$$V_{DI} = -\frac{1}{c(\mu(x_k))(1 - k_E)} \left(M(D, \mu^{(0)}, \phi^{(0)}) \frac{d\mu^{(0)}}{dx} \right) \tag{5.26}$$

The preceding negative sign gets cancelled by negative $\frac{d\mu^{(0)}}{dx}$

5.5 General Conclusions

The solute trapping phenomenon during rapid solidification has been modelled using the phase-field method. We reproduce the work of Wheeler et. al. to show the transition to completely diffusionless transformation does not occur at finite interface velocity. In order to capture the kinetics of rapid solidification, we successfully modify the flux to hyperbolic type in the phase-field model. This allows us to show the transition to diffusionless transformation occurring at a finite interface velocity. Trapping in the Grand Potential phase field model at high solidification velocity has also studied, and has been shown to be naturally contained in the model.

Trapping is quantified by the partition coefficient, a quantity traditionally defined in the sharp interface limit. We also address the fact that trapping depends on the definition of the partition coefficient k in a diffuse interface setting. We use two such definitions in GP model and present a comparison for it. For the choice of partition coefficient k_2 as defined in Eq(4.16) we show its absolute convergence to unity.

We have also simulated the dependency of trapping on the choice of diffusivity interpolation function. We have considered three interpolation functions and plotted the trapping behaviour using each of these for both choices of partition coefficient.

It has been shown that trapping behaviour would depend on interpolation function on one choice of partition coefficient(k_1). The partition coefficient defined by us is independent of the interpolation function. However, completely diffusionless transformation is not represented by $k = 1$ in this setting.

In the end we have performed a asymptotic analysis for chemical potential as a verification of our simulation. The analysis is also used to show the dependence of interface width on the trapping behaviour, where trapping is shown to increase with increasing interface width. The analysis is also used to determine the characteristic velocity V_{DI} which bears significance in understanding solidification cracking during additive manufacturing.

5.6   Future scope of work

Future scope of work would include solidification of dendritic morphologies at high interface velocities. MD simulations dedicated to understanding dynamics at the rapidly solidifying interface would also help us to make better changes to the model. The phase field crystal method could also serve as an alternative tool in this regard.

Appendix A

Hyperbolic flux

Hyperbolic flux equation in steady state is given by,

$$D \left(1 - \frac{V^2}{V_D^2}\right) \frac{d^2 J}{dx^2} + V \frac{dJ}{dx} = 0 \tag{A.1}$$

Integration gives,

$$J(x) = c_1 + c_2 \exp\left(-\frac{V}{D\left(1 - V^2/V_D^2\right)}\right) \tag{A.2}$$

For the interface at x=0

$$J(x) = V\left(c_L^i - c_S^i\right) \exp\left(-\frac{V}{D\left(1 - V^2/V_D^2\right)}\right), \quad V < V_D$$
$$J(x) = 0, \quad V \geqslant V_D \tag{A.3}$$

c_L^i and c_S^i are the liquid and solid compositions at the interface respectively. Using results in Galenko [13]

$$J = -\overline{D} \frac{\partial(\Delta\mu)}{\partial x} - \tau_D \frac{\partial J}{\partial t} \tag{A.4}$$

we get,

$$J = -D \left(\frac{\partial(\Delta\mu)}{\partial c}\right)^{-1} \frac{d(\Delta\mu)}{dx} + D \frac{V^2}{V_D^2} \frac{dc}{dx} \tag{A.5}$$

Thus,

$$J = -D \left(\frac{\partial (\Delta \mu)}{\partial c} \right)^{-1} \left[1 - \frac{V^2}{V_D^2} \right] \frac{d(\Delta \mu)}{dx} \tag{A.6}$$

which for our choice of free-energy becomes,

$$J = -D \left(c \left(1 - c \right) \right) \left[1 - \frac{V^2}{V_D^2} \right] \frac{d(\Delta \mu)}{dx} \tag{A.7}$$

Appendix B

Material parameters in double well Grand Potential

With the interface mobility M as the proportionality constant between velocity and driving force the time scale becomes $\tau = \delta/M$. The fixation of the length scale δ follows from the definition of the interfacial energy. At equilibrium $\Delta F{=}0$ the only energy contribution in the system is the interfacial energy per unit area σ

This is given by,

$$
\begin{aligned}
\sigma &= \int_{-\infty}^{\infty} \mathrm{d}x \left[\frac{\epsilon}{2}(\nabla\phi)^2 + \frac{\gamma}{4}\phi^2(1-\phi)^2 \right] \\
&= \int_0^1 \mathrm{d}\phi \left[\frac{\mathrm{d}x}{\mathrm{d}\phi} \left(\frac{18\epsilon}{\delta^2} + \frac{18\epsilon}{\delta^2} \right) \phi^2(1-\phi)^2 \right] \\
&= \int_0^1 \mathrm{d}\phi \frac{6\epsilon}{\delta}\phi(1-\phi) = \frac{\epsilon}{\delta} = \frac{\delta\gamma}{72}
\end{aligned}
\tag{B.1}
$$

Thus summarizing the results as

$$
\epsilon = \sigma\delta, \quad \gamma = 72\frac{\sigma}{\delta}, \quad \tau = \frac{\delta}{M_\phi}
\tag{B.2}
$$

Bibliography

[1] Monte carlo modeling of dopant segregation. *Journal of Crystal Growth*, 271(3):495 – 512, 2004.

[2] N. A. Ahmad, A. A. Wheeler, W. J. Boettinger, and G. B. McFadden. Solute trapping and solute drag in a phase-field model of rapid solidification. *Phys. Rev. E*, 58:3436–3450, Sep 1998.

[3] Jean-Louis Auriault, Jolanta Lewandowska, and Pascale Royer. About Non-Fickian Hyperbolic Diffusion. In *18ème Congrès Français de Mécanique*, Actes du 18ème Congrès Français de Mécanique, Grenoble, France, August 2007.

[4] Michael J Aziz and Theodore Kaplan. Continuous growth model for interface motion during alloy solidification. *Acta Metallurgica*, 36(8):2335 – 2347, 1988.

[5] J.C. Baker and J.W. Cahn. in solidification, edited by t. j. hughel and g. f. bolling american society of metals, metals park, oh, 1971, p. 23.

[6] H. Biloni and B Chalmers. *Trans. Soc. Min. Eng.*, 233, 1965.

[7] W. J. Boettinger, J. A. Warren, C. Beckermann, and A. Karma. Phase-field simulation of solidification. *Annual Review of Materials Research*, 32(1):163–194, 2002.

[8] Long-Qing Chen. Phase-field models for microstructure evolution. *Annual Review of Materials Research*, 32(1):113–140, 2002.

[9] Abhik Choudhury and Britta Nestler. Grand-potential formulation for multi-component phase transformations combined with thin-interface asymptotics of the double-obstacle potential. *Phys. Rev. E*, 85:021602, Feb 2012.

[10] Stephen J. Cook and Paulette Clancy. Impurity segregation in lennard-jones a/ab heterostructures. i. the effect of lattice strain. *The Journal of Chemical Physics*, 99(3):2175–2191, 1993.

[11] D. Danilov and B. Nestler. Phase-field modelling of solute trapping during rapid solidification of a si–as alloy. *Acta Materialia*, 54(18):4659 – 4664, 2006.

[12] K. Eckler, R. F. Cochrane, D. M. Herlach, B. Feuerbacher, and M. Jurisch. Evidence for a transition from diffusion-controlled to thermally controlled solidification in metallic alloys. *Phys. Rev. B*, 45:5019–5022, Mar 1992.

[13] Peter Galenko. Solute trapping and diffusionless solidification in a binary system. *Phys. Rev. E*, 76:031606, Sep 2007.

[14] Alain Karma. Phase-field formulation for quantitative modeling of alloy solidification. *Phys. Rev. Lett.*, 87:115701, Aug 2001.

[15] Seong Gyoon Kim, Won Tae Kim, and Toshio Suzuki. Interfacial compositions of solid and liquid in a phase-field model with finite interface thickness for isothermal solidification in binary alloys. *Phys. Rev. E*, 58:3316–3323, Sep 1998.

[16] Ryo Kobayashi. Modeling and numerical simulations of dendritic crystal growth. *Physica D: Nonlinear Phenomena*, 63(3):410 – 423, 1993.

[17] Ralf Metzler and Albert Compte. Stochastic foundation of normal and anomalous cattaneo-type transport. *Physica A: Statistical Mechanics and its Applications*, 268(3):454 – 468, 1999.

[18] I. S. Miroshnichenko. Quenching from the liquid state metallurgiya, moscow, 1982.

[19] W.T. Olsen and R Hultgreen. *AIME*, 188, 1950.

[20] S. L. Sobolev. Effects of local non-equilibrium solute diffusion on rapid solidification of alloys. *physica status solidi (a)*, 156(2):293–303.

[21] S.L. Sobolev. Nonlocal diffusion models: Application to rapid solidification of binary mixtures. *International Journal of Heat and Mass Transfer*, 71:295 – 302, 2014.

[22] A. A. Wheeler, W. J. Boettinger, and G. B. McFadden. Phase-field model for isothermal phase transitions in binary alloys. *Phys. Rev. A*, 45:7424–7439, May 1992.

[23] Yang Yang, Harith Humadi, Dorel Buta, Brian B. Laird, Deyan Sun, Jeffrey J. Hoyt, and Mark Asta. Atomistic simulations of nonequilibrium crystal-growth kinetics from alloy melts. *Phys. Rev. Lett.*, 107:025505, Jul 2011.